Acta Pharmaceutica Sinica B 2020;10(10):1977–1988

Chinese Pharmaceutical Association
Institute of Materia Medica, Chinese Academy of Medical Sciences

Acta Pharmaceutica Sinica B

www.elsevier.com/locate/apsb
www.sciencedirect.com

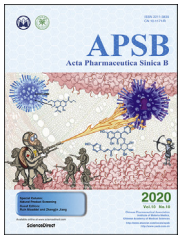

ORIGINAL ARTICLE

Enhanced stability and efficacy of GEM-TOS prodrug by co-assembly with antimetastatic shell LMWH-TOS

Rong Guo[†], Yang Long[†], Zhengze Lu, Miao Deng, Penghui He, Man Li[*], Qin He[*]

Key Laboratory of Drug Targeting and Drug Delivery Systems of the Education Ministry, West China School of Pharmacy, Sichuan University, Chengdu 610064, China

Received 15 April 2019; received in revised form 8 June 2019; accepted 20 June 2019

KEY WORDS

Gemcitabine;
TOS;
LMWH;
Tumor metastasis;
MMP-9

Abstract Chemotherapy agents have been widely used for cancer treatment, while the insolubility, instability and toxicity seriously restrict their efficacy. Thus, prodrug strategy was devised. Since some prodrugs are still with poor solubility or stability, a synergy strategy is needed to enhance their efficacy. Gemcitabine (GEM) is a prescribed anticancer drug, however, the rapid clearance, growing resistance and serious side effects limit its clinical efficacy. Conjugating GEM with D-α-tocopherol succinate (TOS) is an effective solution, while the GEM-TOS (GT) is unstable in aqueous solution. D-α-Tocopherol polyethylene glycol succinate (TPGS) has been used to enhance the stability, but GT stabilized by TPGS (GTT) has limited effect on tumor metastases. Tumor metastases lead to high mortality in patients suffering from cancers. In order to further achieve antimetastatic effect, an amphiphilic polymer (LT) was synthesized by connecting low-molecular-weight heparin (LMWH) with TOS, and eventually obtained desired self-delivery micellar NPs (GLT) by co-assembly GT with LT. The GLT not only possessed excellent stability, but also inhibited the metastases by acting on different phases of the metastatic cascade. The hydrophobic TOS inhibited the secretion of matrix metalloproteinase-9 (MMP-9), the hydrophilic LMWH inhibited the interaction between tumor cells and platelets. As a result, GLT reduced tumor cells entering the blood and implanting at the distant organs, leading to a much more excellent inhibitory effect on the lung metastasis than GEM and GTT.

*Corresponding authors.
E-mail addresses: manli@scu.edu.cn (Man Li), qinhe@scu.edu.cn (Qin He).
[†]These authors made equal contributions to this work.

https://doi.org/10.1016/j.apsb.2019.06.008

1. Introduction

Cancer is a highly malignant disease, which is one of the leading causes of mortality worldwide. During the last several decades, a large number of potent chemotherapy agents have been widely used in clinical cancer treatment. However, the insolubility, instability and toxicity of most chemotherapy agents limit their efficacy. In order to enhance the anticancer effect, the prodrug strategy has been widely devised[1−4]. Prodrugs can be degraded at specific conditions, for example, with the help of carboxylesterases localized in tissues[5], to release the active drugs. However, some prodrugs still have low efficacy due to the poor solubility or stability[6], a synergy strategy which can enhance their efficacy is urgent. Gemcitabine (GEM) is a nucleoside inhibitor commonly used in the clinical treatment of malignant tumors, such as the breast cancer[7−9]. Nevertheless, the use of GEM is usually accompanied with serious side effects. In addition, GEM is easily deaminated to inactive form due to the reactive amino group, leading to a very short plasma half-life[10,11]. To increase its antitumor activity, prodrug strategies have been explored by conjugating hydrophilic GEM with hydrophobic fatty acids on its 4-amino group[12−14]. D-α-Tocopherol succinate (TOS), one of the effective analogues of vitamin E, was reported to be connected with GEM through amide bond[15,16]. The obtained prodrug GEM-TOS (GT) can be degraded in lysosomal acid environment with the presence of cathepsin B, an enzyme which plays a key role in degradations of amide-bearing drugs inside the cells[10]. While the GT are usually unstable in aqueous solution. TPGS is a stabilizer approved by the FDA, it has been selected to improve the stability of GT apparently[11,15,16], but the GT stabilized by TPGS (GTT) has limited effect on tumor metastases.

For patients suffering from cancers, although the growth of primary tumors can be inhibited by surgery, chemotherapy and radiotherapy, the formation of distant metastases still leads to most cancer-related mortality[17,18]. In order to further enable the drug delivery system of GT with antimetastatic ability, preparing a polymer that can not only stabilize the prodrug GT, but also inhibit tumor metastases, could be an effective method. The formation of metastases in distant organs is the consequence of metastatic cascade: tumor cells detach from the primary tumor and penetrate the basement membrane, then enter the circulatory, finally, extravasate and colonize at distant organs to form a secondary tumor[19,20]. Thus, effectively inhibiting the metastatic cascade would be beneficial to cancer treatment.

There are abundant researches indicating that MMP-9 secreted by tumor cells can degrade the extracellular matrix and facilitate tumor cells migrate into blood vessels[21−23]. Our previous study proved that TOS could significantly inhibit the expression of MMP-9[24]. That means TOS can inhibit the first step of the metastatic cascade and inhibit tumor cells entering into blood. Moreover, abundant experimental evidence has also proved that platelets could support tumor metastases by adhering to tumor cells. The adhesion put "platelet coats" on the tumor cells to guard the cells from flow shear stress and immune elimination in blood vessels, assisting tumor cells to cross the blood vessel endothelium[24−26]. LMWH, a degradation product of heparin, has been demonstrated effective on tumor metastases recently[27−29]. LMWH can inhibit the adhesion between platelets and tumor cells, thus inhibiting the subsequent step of the metastatic cascade and decreasing circulating tumor cells (CTCs) implanting at distant organs. Based on the above, an antimetastatic "protecting shell" LT which has effect on different phases of the metastatic cascade was constructed by connecting TOS with LMWH.

In this study, prodrug GEM-TOS (GT) and amphiphilic polymer LMWH-TOS (LT) were synthesized and characterized, respectively, through which we prepared self-delivery micellar NPs (GLT) with excellent stability to achieve both anti-tumor and anti-metastases efficacy. The cytotoxicity and anti-migration effect of GLT were tested on 4T1 cells. The inhibitory effect of GLT on the tumor cell-platelet adhesion was investigated *in vitro*. And the inhibitory effect of GLT on the MMP-9 secretion was investigated on 4T1 cells and 4T1 solid tumors, respectively. In addition, the anti-tumor and anti-metastasis efficacy of GLT were evaluated on 4T1 tumor-bearing mice. The stability and antimetastatic efficacy of GLT were due to the existence of antimetastatic "protecting shell" LT, and the LT synthesized here is promising to stabilize other prodrugs and enhance their antimetastatic efficacy.

2. Methods

2.1. Preparation and characterization of GLT micellar NPs

4.375 mg LT (prepared as in Supporting Information Experimental Section) was dissolved in 5 mL ultrapure water, and then 1 mL GT solution (prepared as in Supporting Information Experimental Section) was added dropwise into it. The GLT micellar NPs were obtained by ultrasonic (80 W, 6 min) and dialyzed with ultrapure water using dialysis membrane (MW 1000) to remove catalysts and the unconnected GEM. The structure of GLT was determined by ^{1}H NMR, IR and MS. In addition, the zeta potential and particle size were measured by Malvern Zetasizer Nano ZS90 (Malvern Instruments Ltd., UK). And the morphology of GLT was observed under a transmission electron microscope (TEM; JEM-100CX, JEOL, Japan).

The content of GEM in GLT was determined by HPLC. GLT was hydrolyzed under the co-catalytic condition of hydrochloric acid and copper chloride (70 °C, 12 h). After filtering to remove the precipitates, samples were analyzed using HPLC equipped with C18 column and UV detector to detect the content of GEM. Ammonium acetate buffer (pH 5.7) and methanol (90:10, *v/v*) were used as mobile phase at a flow rate of 1 mL/min. The detection wavelength was 268 nm.

The content of LMWH in LT and GLT was determined by toluidine blue spectrophotometry. LMWH can be combined with

toluidine blue to obtain a purple complex in PBS (pH 7.4), which can be extracted by hexane. The absorption of aqueous layer (at 630 nm) is linear with the concentration of LMWH when the concentration is low. Briefly, 2.5 mL LT and GLT (40 μg/mL) were mixed with 2.5 mL 0.005% toluidine blue respectively, shaken for 30 s immediately. Then 5.0 mL hexane was added and shaken for another 1 min. After settling down for a while, the aqueous layer was separated to detect the absorption at 630 nm.

2.2. *In vitro drug release study*

In order to investigate *in vitro* GEM release from GLT, GLT was dissolved in PBS with different pH values (pH 7.4, 6.8 and 5.0) and PBS (pH 5.0) containing cathepsin B (0.5 UN/mL), respectively[30], with the final GLT concentrations of 0.1 mg/mL. The solution was incubated at 37 °C, 120 rpm (IS-RDD3, Incushaker, Crystal Technology & Industries, Inc., Taxes, USA). 100 μL solution of each group was taken out and filtrated with 0.22 μm membrane filter at 1, 2, 4, 8, 12, 24 and 48 h. HPLC was used to determine the content of GEM as mentioned before.

2.3. *In vitro stability of GLT*

The stability of GLT was investigated in different medium. Briefly, 500 μL of GLT (1 mg/mL) was mixed with 500 μL 20% FBS, FBS, PBS and RPMI 1640 medium, respectively, and incubated at 37 °C, 75 rpm. Particle size and absorbance at 750 nm were recorded at 0, 1, 2, 4, 8, 12 and 24 h. The changing rate of particle size and transmittance were calculated, and less than 10% changing rate was deemed as stable.

In order to further investigate the long-term stability, GEM-TOS stabilized with TPGS (GTT) was prepared as a control. Briefly, 3.4 mg TPGS was dissolved in 5 mL ultrapure water. Then 1 mL solution of GEM-TOS (prepared as in Supporting Information) was added dropwise into it. The GTT micellar NPs were obtained by ultrasonic (80 w, 6 min) and dialyzing with ultrapure water using dialysis membrane (MW 1000). Both GLT and GTT solution (0.5 mg/mL) were stored at 4 °C. The appearance and particle size are recorded until there is precipitation.

2.4. *Cellular uptake assay*

The uptake of GT and GLT by the 4T1 cells were measured by the HPLC. 2.5×10^5 cells were seeded in 6-wells plate and incubated overnight, and then the culture medium was replaced by 2 mL of fresh medium containing GT or GLT (GEM-equivalent 1 μg/mL). After the incubation for 0.5 and 1 h, the culture medium was removed. Cells were washed with PBS for 3 times and then lysed with 1% SDS. The cells lysates were freeze-dried and dissolved by 200 μL of the mixture of methanol and acetonitrile (1:1, *v/v*). After filtrating with 0.22 μm membrane filter, the concentration of GEM-TOS was determined by HPLC. The mobile phase consisted of ammonium acetate buffer (pH 5.7) and methanol (95:5, *v/v*). The detection wavelength was 268 nm.

2.5. *Scratch healing assay*

Scratch healing assay was performed to investigate whether GLT can inhibit the migration of tumor cells *in vitro*. Briefly, 4T1 cells were seeded into 6-well plates and incubated to near confluence (90%). The cell layer was scratched a straight line, and then washed with PBS and incubated with medium containing PBS, LMWH, GEM and GLT (GEM-equivalent 0.1 μg/mL), respectively, for 12 h. Images were obtained at 0 and 12 h. The scratch-healing rate was calculated by Image J (National Institute of Health, Bethesda, MD, USA).

2.6. *Detection of MMP-9 by Western blot assay*

To investigate whether TOS has inhibitory effect on MMP-9 in 4T1 cells, we detected the MMP-9 by Western blot assay. 4T1 cells were seeded into 6-well plates and incubated to near 60% confluency. Then, the culture medium was replaced with 2 mL of fresh medium containing PBS, LMWH or LT, respectively, for 24 h. After that, 4T1 cells were lysed and centrifuged (15,700×*g*, 4 °C) for 15 min. The supernatant proteins were then separated by 6% SDS-PAGE, followed by transferred to polyvinylidene difluoride membranes. Finally, samples were incubated with antibody. HRP-labeled mouse anti-goat secondary antibody was added and measured using a Bio-Rad ChemiDoc MP System (Bio-Rad Laboratories, Hercules, CA, USA).

2.7. *Interaction of tumor cells with platelets*

4T1 cells were seeded in 6-well plates and grew to approximately 80% confluency. Then the medium was changed and incubated with fresh medium containing PBS, GEM, LMWH, LT or GLT (LMWH-equivalent 80 μg/mL), respectively, for 20 min. Meanwhile, platelets collected from fresh blood were washed with PBS and labeled with 5 μmol/L calcein AM. Twenty minutes later, fluorescein-labeled platelets were added to each well and cultured for another 2 h. After that, the cells were washed with PBS and lysed with DMSO. Finally, the fluorescence signal was detected using a Varioskan Flash Multimode Reader (Thermo Fisher Scientific, Waltham, MA, USA) at Ex = 490 nm and Em = 515 nm.

2.8. *In vivo tumor-targeting assay and biodistribution*

BALB/c female mice (about 5-week-old, 18−22 g, specific pathogen free) were purchased from Dashuo Experimental Animal Company (Chengdu, China). All animal experiments were performed according to the rules of Experimental Animals Administrative Committee of Sichuan University.

The 4T1 solid tumor model was generated by inoculating 1×10^6 4T1 cells on the mammary pad of female BALB/c mice. *In vivo* biodistribution experiment was performed on the tumor-bearing mice at day 10 after the injection of 4T1 cells. The GLT were labeled with DiD *via* physical entrapment. Briefly, GLT and DiD were dissolved in dichloromethane and stirred at 37 °C for 3 h. Then, add the mixture to five volumes of PBS, sonicate (80 w, 6 min) and finally remove dichloromethane by rotary evaporation. As a control, free DiD was dissolved in a mixed solvent of propylene glycol and PBS (1:1, *v/v*)[31]. The tumor-bearing BALB/c mice were randomly divided into 3 groups (n = 9) and injected with PBS, GLT/DiD and free DiD (20 μg DiD per mouse) through the tail vein, respectively. Then, the tumor regions of mice were imaged using an *in vivo* imaging system (IVIS Lumina Series III, PerkinElmer, CA, USA) at 1, 4, 8, 12 and 24 h. In addition, mice were sacrificed at 4, 8 and 24 h, respectively (3 mice for each time point), to collect tumors and major organs for *in vitro* imaging. The frozen sections of tumors at 24 h were observed by laser scanning confocal microscope (FV1000, Olympus, USA) to confirm the distribution of GLT in the tumor site.

2.9. *In vivo anti-tumor assay*

The 4T1 solid tumor model was generated by inoculating 1×10^6 4T1 cells on the mammary pad of female BALB/c mice. Then, the 4T1 tumor-bearing mice were randomly divided into 5 groups ($n = 6$) and injected with PBS, free LMWH, free GEM, GTT and GLT (GEM-equivalent 4 mg/kg, LMWH-equivalent 18.4 mg/kg), respectively, through the tail vein from the day 5 after tumor implantation. Each formulation was administered every 2 days for 5 times. Tumor growth and body weight were recorded during the treatment. And the tumor volume was calculated using ($L \times W^2/2$), in which W was the smaller diameter and L was the larger diameter. At day 18, the mice were sacrificed, and tumors were obtained and imaged. In addition, the tumors and major organs were collected for hematoxylin and eosin (H&E) staining. To further investigate the *in vivo* inhibitory effect of the preparations on the MMP-9, the tumors from mice of each group were applied for immunohistochemical staining. Moreover, tumors from each group were cut into 100-mg pieces, homogenized, and proteins were collected. The expression of MMP-9 in tumors was further determined by Western blot assays as mentioned before.

2.10. *In vivo anti-metastasis activity*

Breast cancer lung metastasis model was established to investigate the anti-metastasis ability of GLT. Briefly, 1×10^6 4T1 cells were injected into the tail vein of female BALB/c mice. Twelve hours later, the mice were randomly divided into 5 groups ($n = 5$) and intravenously injected with PBS, free LMWH, free Gem, GTT and GLT, respectively (GEM-equivalent 4 mg/kg, LMWH-equivalent 18.4 mg/kg). Each formulation was administered every 2 days for 5 times. Body weights of mice were monitored. At day 18, the mice were sacrificed, lungs were obtained and imaged, and the nodules on the surfaces of lungs were counted carefully. In addition, major organs (heart, liver, spleen, lung and kidney) gained from mice of each group were applied for hematoxylin and eosin (H&E) staining. The lungs were also applied for immunohistochemical staining to investigate the effect of the preparations on MMP-9.

2.11. *Pharmacokinetic assay*

The *in vivo* pharmacokinetic study was performed on female BALB/c mice. The mice were injected with GEM and GLT (GEM-equivalent 4 mg/kg), respectively, *via* the tail vein ($n = 6$). Approximately 200 μL of blood samples were withdrawn from the retro-orbital plexus of the mouse eye at various times (5 min, 15 min, 30 min, 1, 2, 4, 8, 12 and 24 h). Blood samples were centrifuged at 4 °C, 2300×g for 10 min. The obtained plasma was diluted 1.5 times with PBS and measured by HPLC. The mobile phase consisted of ammonium acetate buffer (pH 5.7) and methanol (95:5, *v/v*). The detection wavelength was 268 nm. The pharmacokinetic data was analyzed by Data and max Statistics (DAS, Shanghai, China).

2.12. *Preliminary safety evaluation*

Tail bleeding assay was used to explore whether the GLT would cause bleeding risk. The mice were divided into 3 groups ($n = 3$) and intravenously injected with PBS, LMWH, and GLT, respectively (LMWH-equivalent 20 mg/kg). Remove 3 mm from the tip of the tail 30 min after the injection and immediately immerse the tail in PBS at 37 °C[32]. The end point was defined as the time taken for complete cessation of bleeding to occur.

Hematological analysis and biochemical analysis of the serum were conducted to evaluate the toxicities of different preparations. The mice were divided into 4 groups ($n = 3$) and intravenously injected with PBS, free GEM, LT and GLT, respectively (GEM-equivalent 4 mg/kg). Each formulation was administered every 2 days for 5 times. After treatment, blood and serum from each group were gained for detection.

3. Results and discussion

3.1. *Characterization of GEM-TOS conjugate, LMWH-TOS conjugate and GLT micellar NPs*

GEM-TOS (GT) was synthesized by connecting GEM with TOS by amide bond, and LMWH-TOS (LT) was synthesized by connecting LMWH with TOS by ester bond. GLT micellar NPs was prepared by co-assembling GT with LT. The structures of products were confirmed by ^{1}H NMR (Supporting Information Fig. S1). In the ^{1}H NMR spectrum of LT (Fig. S1D), there were characteristic peaks of LMWH and TOS, while the peak of carboxyl (12.314 ppm) disappeared, which indicated LT was synthesized successfully through the ester bond. In addition, in the ^{1}H NMR spectrum of GT (Fig. S1E), the peaks of carboxyl (12.314 ppm) and amino group (8.722 ppm) disappeared, and a peak appeared at 11.235 ppm, which indicated GT was synthesized successfully through the amide bond. In the ^{1}H NMR spectrum of GLT (Fig. S1F), the characteristic absorption peaks of GEM, TOS and LMWH appeared.

The structures of products were also confirmed by IR (Supporting Information Figs. S2−S4). In the IR spectrum of GEM (Fig. S2A), the bands found at 1674 and 1622 cm^{-1} attributed to a characteristic amine bending vibrations. In the IR spectrum of TOS (Fig. S2B), a characteristic band at 1751 cm^{-1} is attributed to the carbonyl group. As for GEM-TOS (Fig. S2C), there was the characteristic carbonyl band at 1745 cm^{-1}, and bands at 1624 and 1571 cm^{-1} represented the amide, which confirmed the formation of amide bond between carboxyl group of TOS and amino group of GEM. In addition, the IR spectrum of LMWH (Fig. S3A) showed characteristic bands at 3438 and 1607 cm^{-1}. As for the LMWH-TOS (Fig. S3C), bands at 1649, 1211 and 995 cm^{-1} confirmed the formation of ester bond. In the IR spectrum of GLT (Fig. S4), there were characteristic bands belong to GEM, TOS and LMWH. The LC–MS spectrum further confirmed the successfully preparation of GLT (Supporting Information Fig. S5).

The particle size and zeta potential of GLT were measured by Malvern Zetasizer Nano ZS90 (Malvern Instruments Ltd., UK). The particle size was 135.8 ± 4.6 nm, PDI = 0.096, and the zeta potential was −34.9 ± 2.3 mV. Micellar NPs observed under a transmission electron microscope (TEM; JEM-100CX, JEOL, Japan) were spherical with uniform size distribution (Fig. 1A). Moreover, the content of GEM in GLT determined by HPLC was 5%. The content of LMWH determined by toluidine blue spectrophotometry was 47% in LT and 23% in GLT.

3.2. *Critical micelle concentration (CMC) of the GLT*

The CMC value is a critical property of micellar NPs which indicates both the polymer's ability to self-assemble in solution and the stability of the micelles once form[33]. A low CMC is necessary for intravenous injection. In this study, pyrene was used as a

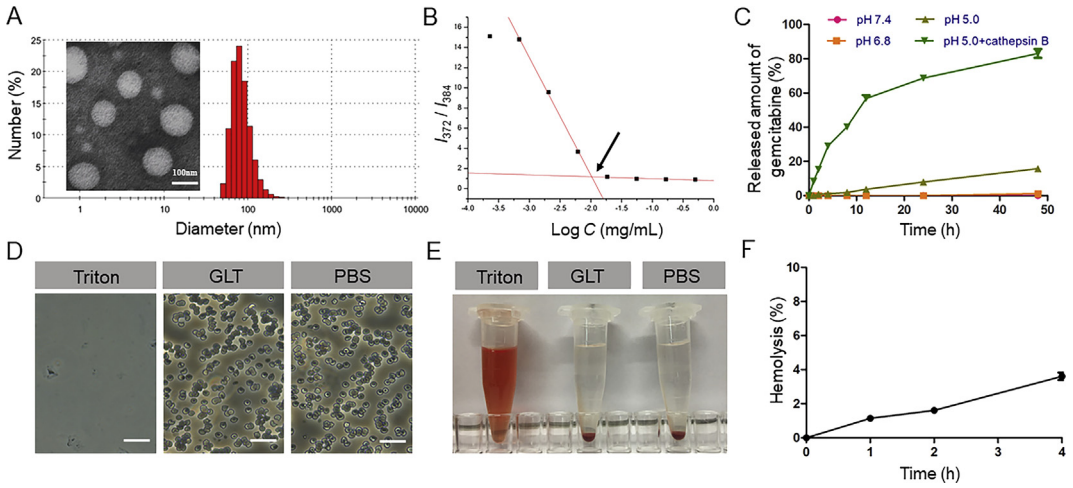

Figure 1 (A) Dynamic light scattering (DLS) size distribution and transmission electron microscopy (TEM) image of GLT. (B) Fluorescence intensity ratio (I_1/I_3) of pyrene as a function of the logarithm of the GLT concentration, CMC is just the concentration of GLT at the intersection. (C) Cumulative GEM release from GLT in different conditions at 37 °C (means ± SD, $n = 3$). (D) Photo images of erythrocytes treated with different formulations (the scale bar represents 25 μm). (E) Images of plastic pipe containing supernatant from red blood cell treated with different formulations. (F) Hemolysis ratio (%) of GLT. A hemolysis ratio less than 5% was regarded as no obvious hemolysis. (means ± SD, $n = 3$).

fluorescence probe, which was sensitive to the polarity change of the environment[34]. Fig. 1B shows the fluorescence intensity ratio (I_1/I_3) of pyrene as a function of the logarithm of the GLT concentration. At low GLT concentrations, pyrene mainly existed in the aqueous solution. As the concentration of GLT increased, pyrene was gradually transferred from the polar aqueous solution to the nonpolar core of the micelles, and thus a substantial decrease in the I_1/I_3 value was observed. The data was fitted into two intersecting lines, and CMC was just the concentration of GLT at the intersection, which was calculated to be 10.3 μg/mL. The results indicated that GLT could withstand the severe dilution, and it would be stable even at a low concentration.

3.3. *In vitro drug release*

In vitro drug release behavior is crucial for drug delivery, and it is necessary for GEM to release from GLT and further achieve the anti-tumor effect. In this study, LMWH was connected with TOS through ester bond, and GEM was connected with TOS through amide bond. Both the ester bond and amide bond were easily degraded in the lysosomal environment. As shown in Fig. 1C, GEM did not significantly release in both pH 7.4 PBS and pH 6.8 PBS, which indicated that GLT could remain stable before cellular uptake. In pH 5.0 PBS, about 16% GEM released after 48 h. However, in pH 5.0 PBS containing cathepsin B, which used to simulate the lysosomal environment, about 80% GEM released after 48 h. The result suggested GEM could be released from GLT in the lysosome, and the drug release behavior was relevant to cathepsin B.

3.4. *Hemolytic activity of GLT*

Blood erythrocytes play an essential role in systemic circulation. However, heparin is an anticoagulant, which may have an enhanced side-effect of hemolysis. Thus, hemolysis assay was conducted to validate the preliminary safety of GLT. As seen in Fig. 1D–F, erythrocytes showed a complete cell lysis when treated with Triton. On the contrary, the hemolysis of GLT was lower than 5% at a concentration of 0.5 mg/mL within 4 h. The microscopic examination and images revealed that the structure of blood erythrocytes had little change and there was no aggregation of erythrocytes after exposure to GLT, which was similar to that treated with PBS (pH 7.4). All these results suggested that GLT had little impact on the integrity of erythrocytes.

3.5. *In vitro stability of GLT*

The stability of GLT in different medium was evaluated respectively. As seen in Fig. 2A and B, GLT remained stable in different medium within 24 h, the changing rates of particle sizes were all less than 10%, and the transmittance of each solution did not change a lot.

The long-term stability of GLT and GTT were investigated by recording their appearance and evaluating their particle size. GTT was used as a control. As seen in Fig. 2C and D, GT was unstable in water and aggregated to form precipitates in 6 h, while the GTT, as reported, was stable without aggregation because of stabilizer TPGS. In this study, a "protecting shell" LT was synthesized to stabilize the GT. It was confirmed that the GLT also remained stable in water until half a year. There was no precipitate formed in GLT, and the sizes did not change a lot. Therefore, LT synthesized here extremely enhanced the stability of GT.

3.6. *In vitro cellular uptake and lysosomal distribution*

Effective uptake of nanoparticles by tumor cells is the premise for their cytotoxicity. The uptake of the GT and GLT were measured by the HPLC. As shown in Fig. 3B, the uptake of GLT at 1 h was higher than that at 0.5 h, and GLT was more efficiently taken up by 4T1 cells than GT. That might because GT was unstable and easy to form precipitates, resulting in a decreased cellular uptake. However, the GLT with excellent stability could pass through cell membrane more easily than GT.

The result of *in vitro* drug release suggested that GEM could release from GLT in lysosomal environment. Therefore, whether GLT reached lysosome after the cellular uptake was critical for its

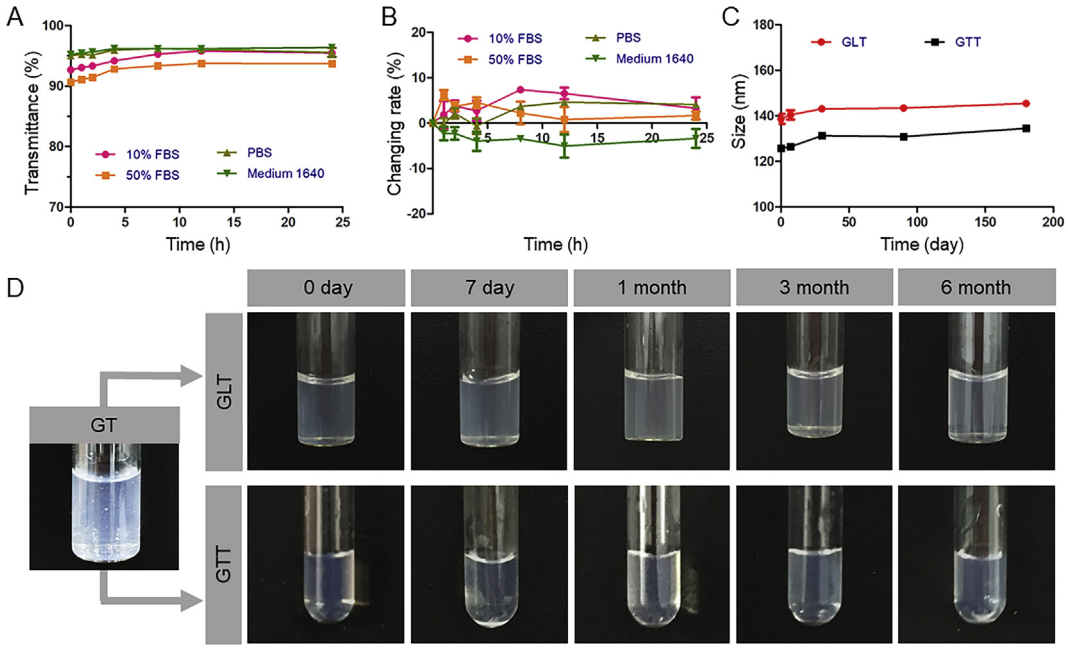

Figure 2 *In vitro* stability of GLT. (A) Changing rates of the particle size during 24 h at 37 °C (means ± SD, $n = 3$). (B) The transmittance of GLT during 24 h at 37 °C (means ± SD, $n = 3$). (C) particle sizes of GLT and GTT in half a year. (D) Images of GLT and GTT in half a year, compared with GT which aggregated to precipitates.

efficacy. As shown in Fig. 3A, there was significant colocalization of GLT and lysosomes at 2 h, which indicated GLT could reach lysosomes after cellular uptake for further drug release.

3.7. *In vitro cytotoxicity and ability to induce apoptosis*

The cytotoxicity was evaluated by determining the viability of cells after incubation with different preparations using the MTT assay. As shown in Fig. 3C, both GEM and GLT had concentration-dependent cytotoxicity. When the concentration of GEM was more than 0.037 μg/mL, free drugs were more cytotoxic than GLT. However, when the concentration of GEM was less than 0.012 μg/mL, GLT was more cytotoxic. This phenomenon might due to the enhanced stability of GEM in micellar formulation against cytidine deaminase, which could convert the GEM to inactive metabolite[14]. The GLT protected GEM from metabolism, and thus it was effective even at a low concentration. At high concentrations, although some of free GEM was metabolized to the inactive form, the remained was sufficient to achieve cytotoxicity. Therefore, free GEM that quickly diffused into the cells was more cytotoxic under that condition. In addition, as shown in Fig. 3D, LT almost did not affect cell viability on 4T1 cells, even at a concentration of 250 μg/mL. The ability of GLT to induce apoptosis was explored by Annexin V-FITC/PI apoptosis detection kit. GLT can induce apoptosis of 4T1 cells at a low concentration of GEM. And there was more apoptosis in the GLT group compared with GEM group (Supporting Information Fig. S9), which was consistent with the result of MTT assay.

3.8. *In vitro inhibitory effect on cell migration*

The migration of tumor cells is directly associated with metastasis[35]. 4T1 cells with strongly metastatic tendency were used to investigate the antimetastatic effect of GLT. In the scratch-healing assay, Fig. 3E and F showed that the scratch in PBS group almost healed after 12 h, with a healing rate of about 90%, and the healing rates decreased when treated with LMWH and GEM. However, it was worth noting that the healing rate was just about 20% after treated with GLT. The results indicated that GLT was able to inhibit the migration of 4T1 cells effectively.

The MMP-9 secreted by tumor cells is closely related to tumor metastasis. Tumor metastasis is a complex process, and the tumor cells need to leave the primary tumor before entering the circulatory and migrating to distant organs[19,20]. MMP-9 had an effect on degrading the extracellular matrix, thus it facilitated tumor cells migrate into blood vessels[21–23]. In our previous study, the secretion of MMP-9 in B16F10 cells was proved to be inhibited by TOS[24]. But the effect of TOS in 4T1 cells is still not clear. Here, the MMP-9 produced by 4T1 cells was detected by Western blot assay. As shown in Fig. 3H, LT significantly inhibited the MMP-9 secreted by 4T1 cells at a concentration of 100 μg/mL, while the free LMWH did not have obvious effect. The result suggested that TOS but not LMWH inhibited MMP-9 expression.

3.9. *In vitro inhibitory effect on the adhesion of platelets to tumor cells*

During the process of metastasis, tumor cells should get the ability to migrate and invade after leaving the primary tumor. The abundant platelets in blood significantly assisted tumor metastasis[24–26]. Thus, it is important to inhibit the adhesion between tumor cells and platelets. *In vitro* assay was conducted here to evaluate whether LMWH or LMWH-based GLT could inhibit the adhesion. As seen in Fig. 3G, LMWH, LT and GLT significantly decreased the number of adhesive platelets on tumor cells compared with PBS group. Tumor cells have been demonstrated to interact with platelets through P-selectin, an adhesion molecule expressed on the surface of activated platelets[36–38]. Therefore,

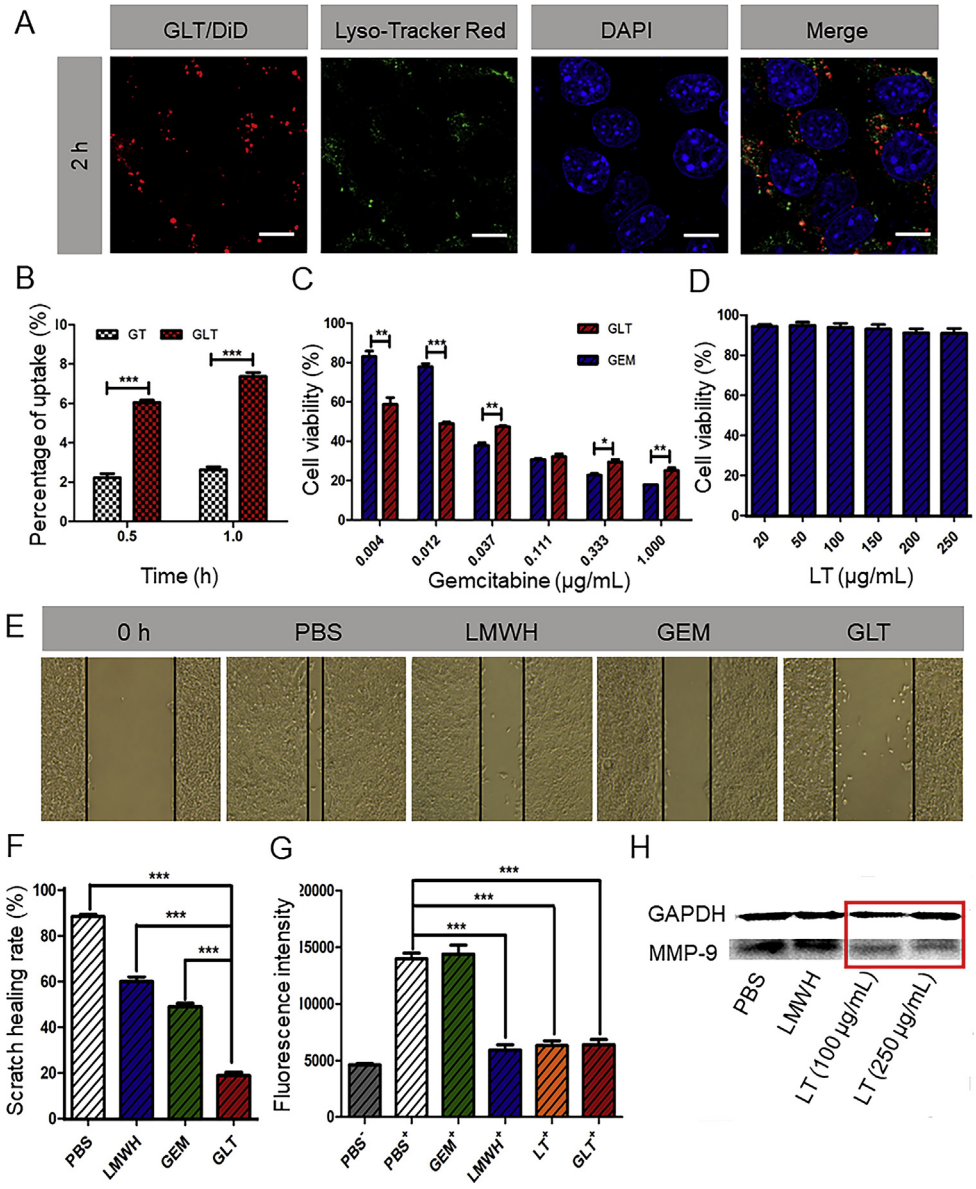

Figure 3 (A) The colocalization of GLT and lysosomes. GLT was labeled with DiD (red), lysosomes were stained with Lyso-Tracker Red (green), and cell nucleuses were stained with DAPI (blue). (B) Cellular uptake of GT and GLT in 4T1 cells (means ± SD, $n = 3$; $^{*}P < 0.05$, $^{**}P < 0.01$ and $^{***}P < 0.001$). (C) Growth inhibitory effect of GEM and GLT on 4T1 cells. (D) Growth inhibitory effect of LT on 4T1 cells (means ± SD, $n = 3$; $^{*}P < 0.05$, $^{**}P < 0.01$ and $^{***}P < 0.001$) (E) Images of scratch after incubation with free GEM, LMWH and GLT, respectively, for 12 h. (F) Scratch healing rates calculated by Image J (means ± SD, $n = 3$; $^{*}P < 0.05$, $^{**}P < 0.01$ and $^{***}P < 0.001$). (G) The fluorescence intensity of platelets adhering to 4T1 cells detected by a Varioskan Flash Multimode Reader (Thermo, USA). "+" indicates coincubation with calcein-AM labeled platelets, "−" indicates no coincubation with calcein-AM labeled platelets (means ± SD, $n = 3$; $^{*}P < 0.05$, $^{**}P < 0.01$ and $^{***}P < 0.001$). (H) Expression of MMP-9 in 4T1 cells tested by Western blot after separate incubation with PBS, LMWH (60 μg/mL), LT (100 μg/mL) and LT (250 μg/mL).

LMWH and GLT might inhibit the tumor cells-platelets adhesion through inhibiting the P-selectin.

3.10. *In vivo tumor-targeting effect*

In vivo tumor-targeting ability of GLT was investigated on the 4T1 tumor-bearing mice. PBS, free DiD and GLT/DiD were injected in different groups ($n = 9$), respectively. The time-dependent biodistribution of DiD was measured, as shown in Fig. 4A and B. The signal of free DiD was mainly showed in liver. However, in tumor region, the fluorescence intensity of the GLT/DiD was higher than that of free DiD at all time points, and the signal of GLT/DiD was strongest at 8 h. The result suggested that GLT had excellent tumor targeting effect. At 4, 8 and 24 h, the mice were sacrificed, the images of organs were obtained (Supporting Information Fig. S10). At 24 h, the fluorescence intensity of GLT/DiD in tumor was 2.5 times as high as that of free DiD (Fig. 4E and F). In addition, in Fig. 4D, the fluorescence of GLT/DiD in lung was obviously much higher than that of free DiD (almost eight times). This might due to the existence of reticuloendothelial system (RES) in the lung, causing some of GLT to retain in the lung.

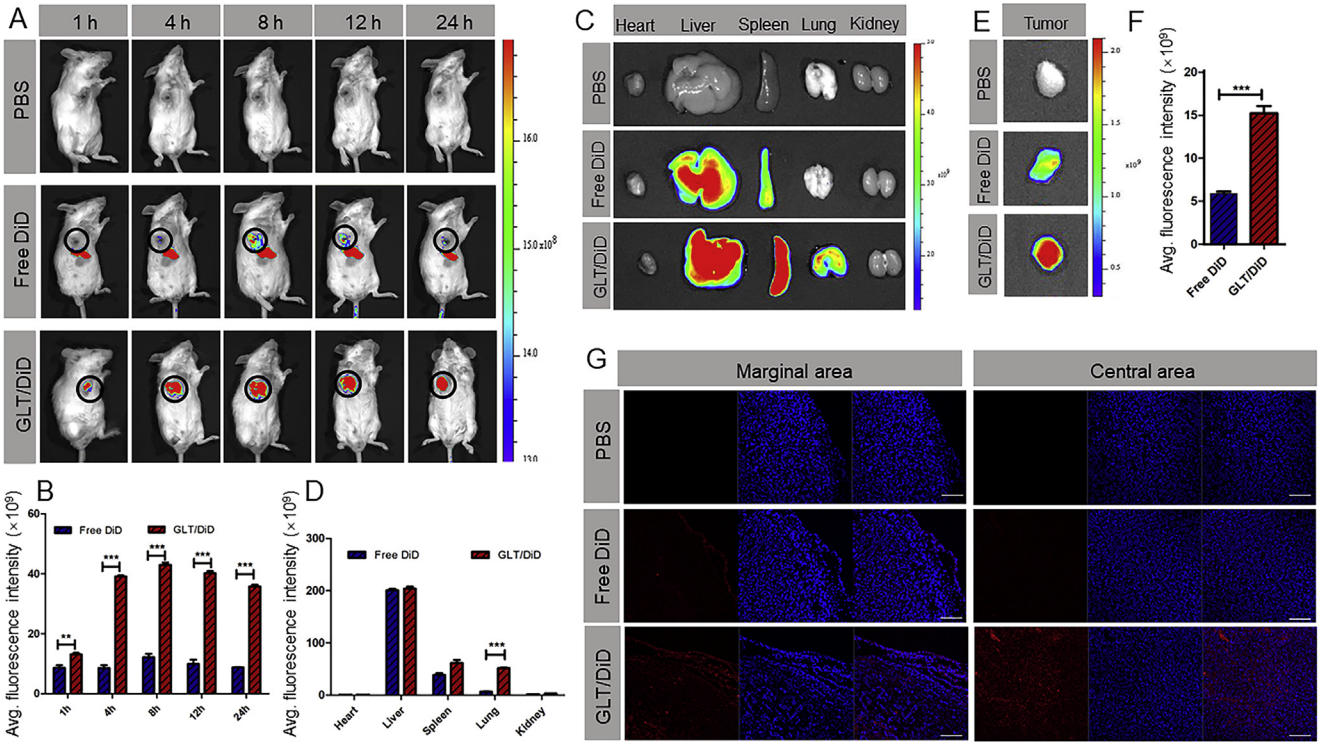

Figure 4 Biodistribution of GLT *in vivo*. (A) *In vivo* images of mice and (B) semiquantitative mean fluorescence intensity results showing the tumor distribution of DiD in 4T1 tumor-bearing mice at 1, 2, 4, 8, 12 and 24 h (mean ± SD, $n = 3$; $^{*}P < 0.05$, $^{**}P < 0.01$ and $^{***}P < 0.001$). (C) *In vitro* images of organs and (D) semiquantitative mean fluorescence intensity results showing the organ distribution of DiD in 4T1 tumor-bearing mice at 24 h (mean ± SD, $n = 3$; $^{*}P < 0.05$, $^{**}P < 0.01$ and $^{***}P < 0.001$). (E) *In vitro* images of tumors and (F) semiquantitative mean fluorescence intensity results showing the tumor distribution of DiD at 24 h (mean ± SD, $n = 3$; $^{*}P < 0.05$, $^{**}P < 0.01$ and $^{***}P < 0.001$). (G) CLSM images of tumor tissue frozen sections from 4T1 tumor-bearing mice 24 h after systemic administration of DiD (red). Cell nucleuses were stained with DAPI (blue). Scale bar indicates 200 μm.

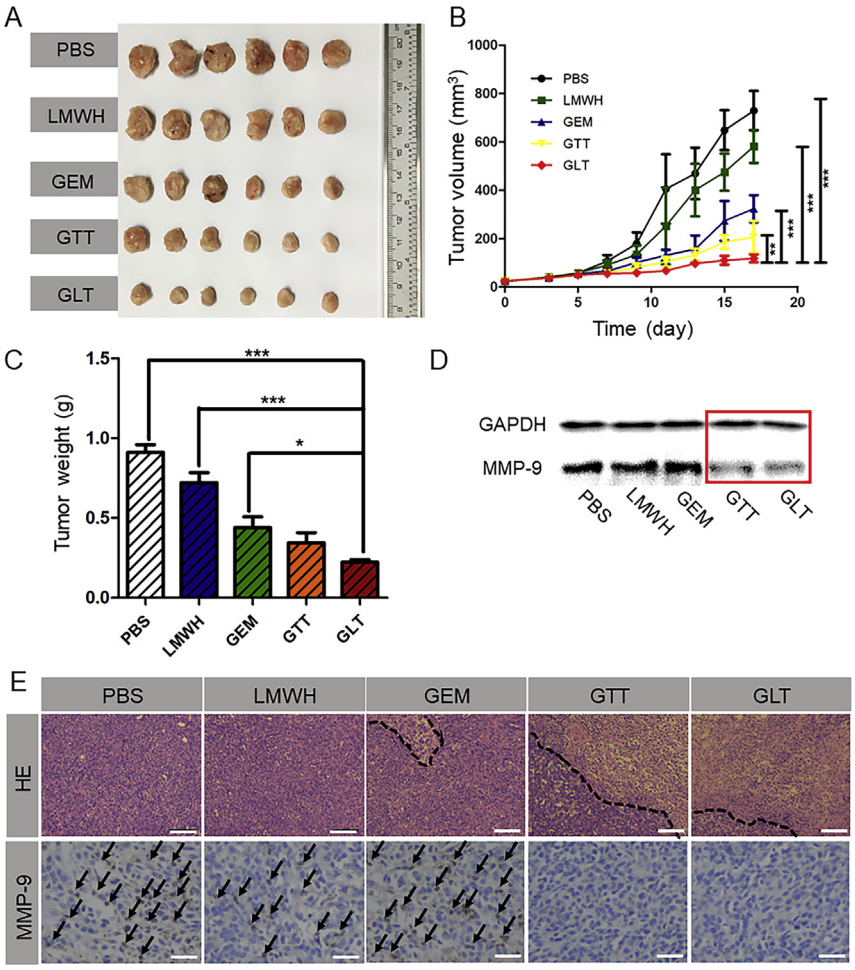

Figure 5 *In vivo* 4T1 solid tumor treatment. (A) Images of 4T1 tumors harvested from BALB/c mice after treatment with PBS, LMWH, free GEM, GTT or GLT, respectively, by intravenous injection. (B) Tumor volume changes in 4T1 tumor-bearing BALB/c mice during the therapies (means ± SD, $n = 6$; $^{*}P < 0.05$, $^{**}P < 0.01$ and $^{***}P < 0.001$). (C) Weights of the harvested 4T1 tumors (means ± SD, $n = 6$; $^{*}P < 0.05$, $^{**}P < 0.01$ and $^{***}P < 0.001$). (D) Expression of MMP-9 in 4T1 tumors tested by Western blot assay. (E) Hematoxylin and eosin (HE) assays for 4T1 tumors (the scale bar represents 100 μm) and immunohistochemical analysis of MMP-9 staining for 4T1 tumors (the scale bar represents 25 μm). The secreted MMP-9 was stained violet and indicated by black arrows.

Tumor targeting effect of GLT was further confirmed by the frozen tumor tissue sections. As shown in Fig. 4G, there were high fluorescence of GLT/DiD in both marginal area and central area at 24 h.

3.11. *In vivo anti-tumor efficacy*

To investigate the *in vivo* antitumor efficacy of GLT, 4T1 cells were inoculated on the mammary pad of female BALB/c mice to establish a tumor-bearing mouse model. They were randomly divided into 5 groups ($n = 6$) and intravenously injected with PBS, free LMWH, free GEM, GTT and GLT, respectively, from the day 5 after tumor implantation. Each formulation was administered every 2 days for a total of 5 times. Tumor volume were recorded (Fig. 5B). The mice were sacrificed on the day 18. Then, the tumors were carefully excised from the mice and weighed. As shown in Fig. 5A–C, the mice treated with PBS, free LMWH and free GEM exhibited rapid tumor growth. Compared with the other groups, both the average tumor weight and the tumor volume in GLT were the smallest. The excellent antitumor efficiency of GLT was due to the stabilization effect of LT, thus allowing more GT to accumulate in the tumor site in the form of micellar NPs.

As shown in Fig. 5E, HE staining showed that tumor treated with PBS and free LMWH retained their complete microstructures. However, extensive tissue necrosis could be observed in GTT and GLT groups, and tumors treated with GLT exhibited a larger area of necrosis, indicating a more efficient antitumor effect. In addition, immunohistochemical analysis suggested that GTT or GLT reduced the secretion of MMP-9 in tumor. The MMP-9 in tumor was also detected by Western blot assay. As seen in Fig. 5D, MMP-9 expression was significantly reduced in 4T1 solid tumors when treated with GTT or GLT, which was similar with the result in immunohistochemical analysis. The results indicated that TOS had an inhibitory effect on MMP-9. Thus, TOS could prevent tumor cells from penetrating blood vessels and inhibit tumor metastases.

3.12. *In vivo anti-metastasis efficacy*

Tumor metastasis model was established *via* the tail vein injection of 4T1 cells, which was used to investigate the *in vivo* anti-

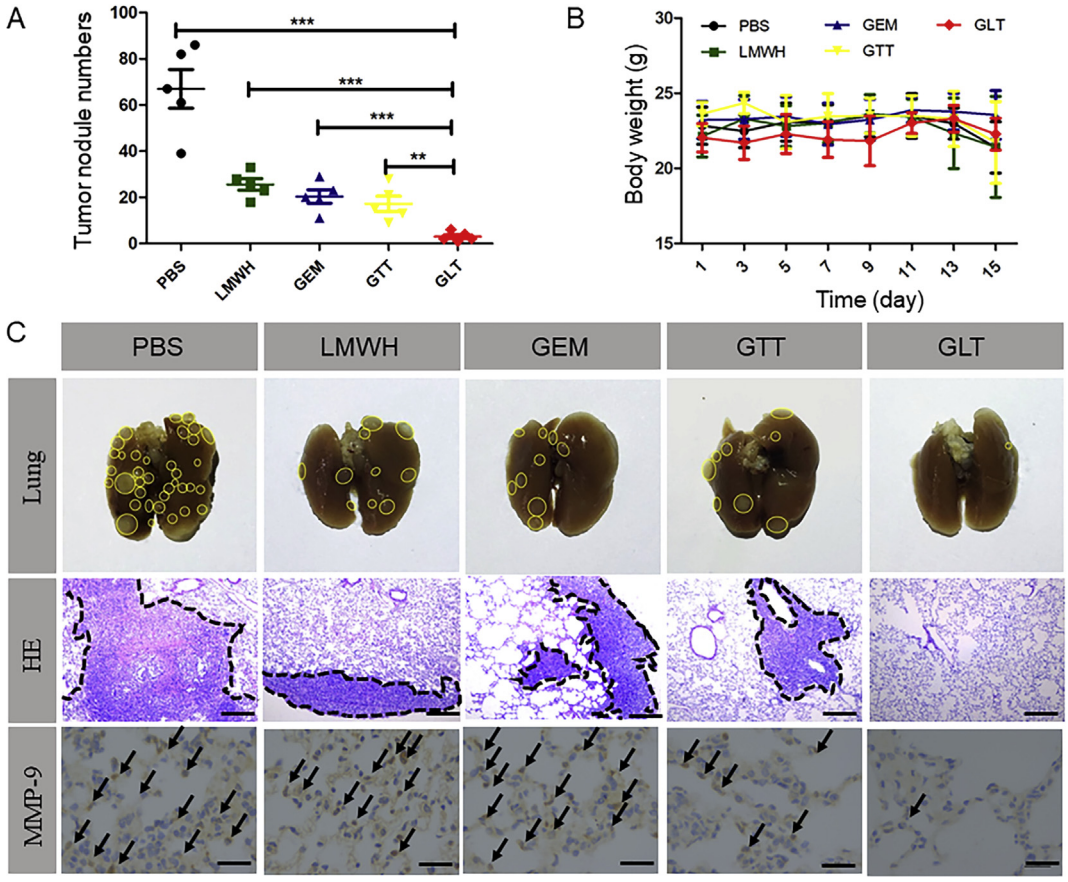

Figure 6 *In vivo* anti-metastasis treatment. (A) The number of 4T1 metastases nodules on the lung surface (means ± SD, $n = 5$; $^{*}P < 0.05$, $^{**}P < 0.01$ and $^{***}P < 0.001$). (B) Body weight of BALB/c mice during the therapies (means ± SD, $n = 5$). (C) Images of lungs, HE staining for lungs (the scale bar represents 100 μm) and immunohistochemical analysis of MMP-9 staining for lungs (the scale bar represents 25 μm) after treatment with PBS, LMWH, free GEM, GTT or GLT, respectively, by intravenous injection. Black arrows indicate the secreted MMP-9.

metastasis activity of GLT. On the day 18, the mice were sacrificed to obtain the lungs, and then the number of metastasis nodules on the surface of lungs were counted carefully (Fig. 6A). In addition, the photos of lungs in Fig. 6C showed that the 4T1 metastasis nodules occupied a majority of the area of the lung tissue in PBS group. Due to the toxicity of free GEM, there were fewer metastasis nodules in GEM group. And the lung metastases decreased in LMWH group because of the inhibition of platelet-

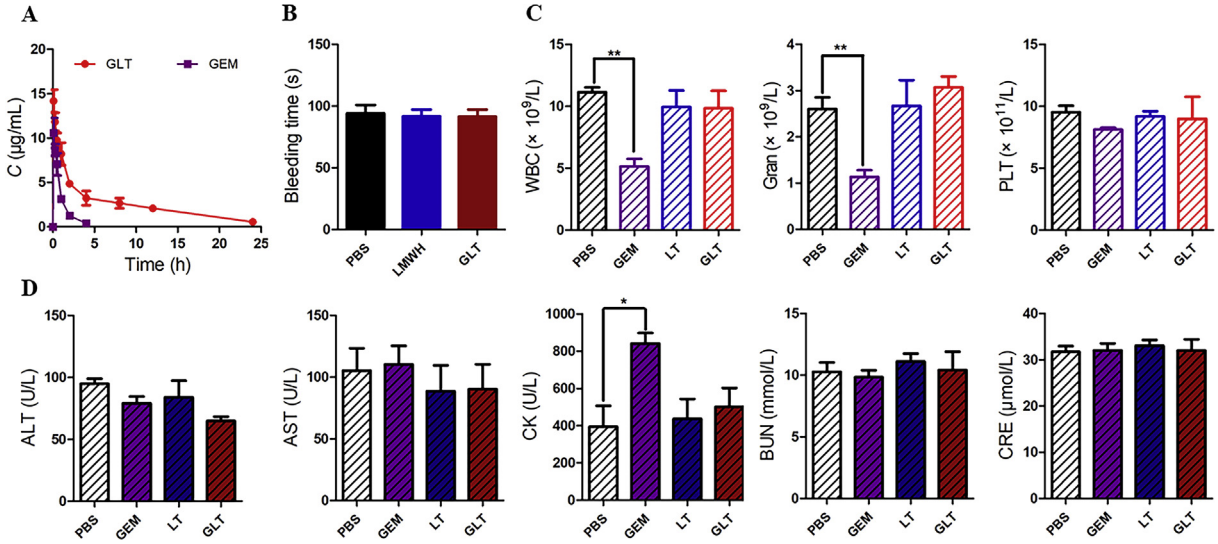

Figure 7 (A) The drug concentration−time curve of GLT and GEM. (B) Bleeding time of BALB/c mice treatment with PBS, LMWH and GLT by intravenous injection (means ± SD, $n = 3$). (C) Blood routine examination and (D) serum biochemistry data of BALB/c mice treated with PBS, free GEM, LT and GLT (at an equivalent dose of 4 mg/kg GEM), respectively, in a total of 5 times (means ± SD, $n = 3$; $^{*}P < 0.05$, $^{**}P < 0.01$ and $^{***}P < 0.001$).

Table 1 Pharmacokinetic parameters after intravenous administration of GEM and GLT ($n = 3$).

Parameter	$t_{1/2}$ (h)	V_1 (L/kg)	CL (L/h/kg)	AUC_{0-t} (mg·h/L)	$AUC_{0-\infty}$ (mg·h/L)
GEM	0.615±0.037	0.027±0.015	0.340±0.085	10.881±2.552	11.241±2.816
GLT	7.632±1.039	0.29±0.056	0.052±0.007	62.648±15.722	82.692±10.514

GEM, gemcitabine; GLT, GEM-TOS co-assembly with LMWH-TOS.

tumor cell adhesion by LMWH. In addition, GTT decreased the number of tumor nodules, but it had no obvious improvement compared with the free GEM. Although GTT was able to inhibit the secretion of MMP-9 in solid tumor, it was obviously not enough to inhibit tumor metastasis completely. As for mice treated with GLT, the nodules were almost invisible. The excellent anti-metastasis efficacy of GLT was mainly due to the "shell" LT, which had effect on different phases of the metastatic cascade. LT was proved to not only inhibited the secretion of MMP-9 in solid tumor, but also prevented tumor cells from adhering to platelets, thereby effectively reducing 4T1 cells implanting at new organs. Combined with the toxicity of GEM, there were few tumor cells could colonize at lung to form tumor nodules.

In Fig. 6C, HE staining also showed similar result. GLT exhibited stronger inhibitory effect on tumor metastasis compared with other groups. Moreover, it was reported that MMP-9 could lead to a proliferative, immunosuppressive and inflamed environment in the lung, which supported the tumor metastases by promoting the implantation of circulating tumor cells[18,39,40]. Immunohistochemical staining of lungs revealed that the expression of MMP-9 in lung was reduced in GLT group, which might have inhibitory effect on tumor cell implantation in lung. The other organs of mice were also stained with HE (Supporting Information Fig. S12). After treatment, myocardial rupture and glomerular effusion could be observed in GEM group, while other groups did not show morphological difference compared with the PBS group.

3.13. *Pharmacokinetic of GLT*

Plasma concentration of GEM was measured using HPLC. The drug concentration−time curve was shown in Fig. 7A. As expected, free GEM showed a higher clearance *in vivo*. And pharmacokinetic parameters in Table 1 indicated that the $AUC_{0-\infty}$ of GEM in GLT (82.692 ± 10.514 mg·h/L) was much higher than that of free GEM (11.241 ± 2.816 mg·h/L), the $t_{1/2}$ of GEM was prolonged by GLT, and GLT significantly decreased the clearance rate of GEM.

3.14. *Preliminary safety of GLT*

Heparin is an anticoagulant, which may enhance the risk of bleeding. LMWH, the composition of GLT, was prepared by depolymerization of heparin. Tail bleeding assay was used to explore whether the GLT would cause bleeding risk. As shown in Fig. 7B, there was no significant difference in bleeding time among three groups. It confirmed that both LMWH and GLT would not cause bleeding risk at this dosage.

Hematological analysis was used to evaluate the toxicities of preparations. As shown in Fig. 7C, compared with the PBS group, GEM treatment resulted in a decrease in the number of white blood cells (WBC) and neutrophilic granulocyte (Gran) in mice. This result suggested that GEM might have side effects of bone marrow toxicity at the dosage. However, mice treated with GLT did not exhibit a similar phenomenon, which indicated that GLT could reduce the toxicity of GEM.

A biochemical analysis of the serum was also used to evaluate organ toxicity (Fig. 7D). Free GEM increased the levels of CK (creatine kinase), which indicated that free GEM could probably cause heart injury. But GLT reduced the injury. The evaluation demonstrated that GLT was biocompatible and safe for injection.

4. Conclusions

In this study, we constructed an antimetastatic "protecting shell" LT successfully to stabilize the prodrug GEM-TOS. The micellar NPs GLT were established by co-assembling GT with LT. It delivered the chemotherapy drug GEM to tumor and avoided the rapid deamination of GEM. The results of long-term stability proved that GLT remained stable in half a year without precipitation, which was comparable with GTT. *In vitro* assays proved that GLT was efficiently taken up by 4T1 cells and it induced apoptosis of 4T1 cells even at a low concentration. Moreover, GLT had excellent inhibitory effect on cell migration. In breast cancer treatment, GLT could accumulate in tumor and inhibit the growth of 4T1 solid tumors effectively. In addition, GLT inhibited the tumor metastasis by acting on different phases of the metastatic cascade. It was proved that GLT decreased the secretion of MMP-9 in 4T1 cells, thus inhibiting tumor cells penetrating the basement membrane and entering the circulatory. GLT also inhibited the interaction between tumor cells and platelets, thus inhibiting tumor cells implanting at distant organs. As a result, GLT showed much more excellent inhibitory effect on the lung metastases than GTT and GEM. In summary, the "protecting shell" LT not only improved the stability of GT, but also endowed the micellar NPs excellent antimetastatic efficacy. The LT is promising to improve the stability and antimetastatic effect of other prodrugs.

Acknowledgments

This work was supported by Major Projects of the National Natural Science Foundation of China (81690261), Sichuan Science and Technology Program (2018RZ0136, China).

Author contributions

Rong Guo, Yang Long and Qin He designed the research. Rong Guo carried out the experiments and performed data analysis. Zhengze Lu, Miao Deng and Penghui He participated part of the experiments. Rong Guo wrote the manuscript. Yang Long, Man Li and Qin He revised the manuscript. All of the authors have read and approved the final manuscript.

Conflicts of interest

The authors have no conflicts of interest to declare.

Appendix A. Supporting information

Supporting data to this article can be found online at https://doi.org/10.1016/j.apsb.2019.06.008.

References

1. Bildstein L, Dubernet C, Couvreur P. Prodrug-based intracellular delivery of anticancer agents. *Adv Drug Deliv Rev* 2011;**63**:3–23.
2. Stella VJ, Nti-Addae KW. Prodrug strategies to overcome poor water solubility. *Adv Drug Deliv Rev* 2007;**59**:677–94.
3. Zheng Y, Ji X, Ji K, Wang B. Hydrogen sulfide prodrugs—a review. *Acta Pharm Sin B* 2015;**5**:367–77.
4. Li N, Cai H, Jiang L, Hu J, Bains A, Hu J, et al. Enzyme-sensitive and amphiphilic PEGylated dendrimer-paclitaxel prodrug-based nanoparticles for enhanced stability and anticancer efficacy. *ACS Appl Mater Interfaces* 2017;**9**:6865–77.
5. Wang D, Zou L, Jin Q, Hou J, Ge G, Yang L. Human carboxylesterases: a comprehensive review. *Acta Pharm Sin B* 2018;**8**:699–712.
6. Mura S, Bui DT, Couvreur P, Nicolas J. Lipid prodrug nanocarriers in cancer therapy. *J Control Release* 2015;**208**:25–41.
7. Zhang J, Wang Z, Hu X, Wang B, Wang L, Yang W, et al. Cisplatin and gemcitabine as the first line therapy in metastatic triple negative breast cancer. *Int J Cancer* 2014;**136**:204–11.
8. Koshy N, Quispe D, Shi R, Mansour R, Burton GV. Cisplatin-gemcitabine therapy in metastatic breast cancer: improved outcome in triple negative breast cancer patients compared to non-triple negative patients. *Breast* 2010;**19**:246–8.
9. Abotaleb M, Kubatka P, Caprnda M, Varghese E, Zolakova B, Zubor P, et al. Chemotherapeutic agents for the treatment of metastatic breast cancer: an update. *Biomed Pharmacother* 2018;**101**:458–77.
10. Immordino ML, Brusa P, Rocco F, Arpicco S, Ceruti M, Cattel L. Preparation, characterization, cytotoxicity and pharmacokinetics of liposomes containing lipophilic gemcitabine prodrugs. *J Control Release* 2004;**100**:331–46.
11. Xu Y, Meng H, Du F, Lu W, Liu S, Huang J, Yu J. Preparation of intravenous injection nanoformulation of VESylated gemcitabine by co-assembly with TPGS and its anti-tumor activity in pancreatic tumor-bearing mice. *Int J Pharm* 2015;**495**:792–7.
12. Zhu S, Lansakara-P DS, Li X, Cui Z. Lysosomal delivery of a lipophilic gemcitabine prodrug using novel acid-sensitive micelles improved its antitumor activity. *Bioconjug Chem* 2012;**23**:966–80.
13. Lee GY, Qian WP, Wang L, Wang YA, Staley CA, Satpathy M, et al. Theranostic nanoparticles with controlled release of gemcitabine for targeted therapy and MRI of pancreatic cancer. *ACS Nano* 2013;**7**:2078–89.
14. Khare V, Al Sakarchi W, Gupta P, Curtis AD, Hoskins C. Synthesis and characterization of TPGS-gemcitabine prodrug micelles for pancreatic cancer therapy. *RSC Adv* 2016;**6**:60126–37.
15. Abu-Fayyad A, Nazzal S. Gemcitabine-vitamin E conjugates: synthesis, characterization, entrapment into nanoemulsions, and *in-vitro* deamination and antitumor activity. *Int J Pharm* 2017;**528**:463–70.
16. Yu J, Meng H, Du F, Huang J, Lu W, Luo Y. Enhanced solubility, stability, and antitumor activity of the VESylated gemcitabine prodrug by co-assembly with TPGS. *J Control Release* 2015;**213**:e48.
17. Mei L, Liu Y, Zhang H, Zhang Z, Gao H, He Q. Antitumor and antimetastasis activities of heparin-based micelle served as both carrier and drug. *ACS Appl Mater Interfaces* 2016;**8**:9577–89.
18. Peinado H, Zhang H, Matei IR, Costa-Silva B, Hoshino A, Rodrigues G, et al. Pre-metastatic niches: organ-specific homes for metastases. *Nat Rev Canc* 2017;**17**:302–17.
19. Chaffer CL, Weinberg RA. A perspective on cancer cell metastasis. *Science* 2011;**331**:1559–64.
20. Jablonska J, Lang S, Sionov RV, Granot Z. The regulation of pre-metastatic niche formation by neutrophils. *Oncotarget* 2017;**8**:112132–44.
21. Kessenbrock K, Plaks V, Werb Z. Matrix metalloproteinases: regulators of the tumor microenvironment. *Cell* 2010;**141**:52–67.
22. Mehner C, Hockla A, Miller E, Ran S, Radisky DC, Radisky ES. Tumor cell-produced matrix metalloproteinase 9 (MMP-9) drives malignant progression and metastasis of basal-like triple negative breast cancer. *Oncotarget* 2014;**5**:2736–49.
23. Hiratsuka S, Nakamura K, Iwai S, Murakami M, Itoh T, Kijima H, et al. MMP9 induction by vascular endothelial growth factor receptor-1 is involved in lung-specific metastasis. *Cancer Cell* 2002;**2**:289–300.
24. Long Y, Lu Z, Mei L, Li M, Ren K, Wang X, et al. Enhanced melanoma-targeted therapy by "Fru-blocked" phenyboronic acid-modified multiphase antimetastatic micellar nanoparticles. *Adv Sci* 2018;**5**:1800229.
25. Labelle M, Begum S, Hynes RO. Direct signaling between platelets and cancer cells induces an epithelial-mesenchymal-like transition and promotes metastasis. *Cancer Cell* 2011;**20**:576–90.
26. Stanger BZ, Kahn ML. Platelets and tumor cells: a new form of border control. *Cancer Cell* 2013;**24**:9–11.
27. Choi JU, Chung SW, Al-Hilal TA, Alam F, Park J, Mahmud F, et al. A heparin conjugate, LHbisD4, inhibits lymphangiogenesis and attenuates lymph node metastasis by blocking VEGF-C signaling pathway. *Biomaterials* 2017;**139**:56–66.
28. Yang X, Du H, Liu J, Zhai G. Advanced nanocarriers based on heparin and its derivatives for cancer management. *Biomacromolecules* 2015;**16**:423–36.
29. Alam F, Al-Hilal TA, Park J, Choi JU, Mahmud F, Jeong JH, et al. Multi-stage inhibition in breast cancer metastasis by orally active triple conjugate, LHTD4 (low molecular weight heparin-taurocholate-tetrameric deoxycholate). *Biomaterials* 2016;**86**:56–67.
30. Han H, Valdepérez D, Jin Q, Yang B, Li Z, Wu Y, et al. Dual enzymatic reaction-assisted gemcitabine delivery systems for programmed pancreatic cancer therapy. *ACS Nano* 2017;**11**:1281–91.
31. Sasatsu M, Onishi H, Machida Y. *In vitro* and *in vivo* characterization of nanoparticles made of MeO-PEG amine/PLA block copolymer and PLA. *Int J Pharm* 2006;**317**:167–74.
32. Wang C, Sun W, Ye Y, Hu Q, Bomba HN, Gu Z. *In situ* activation of platelets with checkpoint inhibitors for post-surgical cancer immunotherapy. *Nat Biomed Eng* 2017;**1**:0011.
33. Glavas L, Olsén P, Odelius K, Albertsson AC. Achieving micelle control through core crystallinity. *Biomacromolecules* 2013;**14**:4150–6.
34. Di Y, Gao Y, Gai X, Wang D, Yang X, Zhang D, et al. Co-delivery of hydrophilic gemcitabine and hydrophobic paclitaxel into novel polymeric micelles for cancer treatment. *RSC Adv* 2017;**7**:24030–9.
35. Kramer N, Walzl A, Unger C, osner M, Krupitza G, Hengstschläger M, et al. *In vitro* cell migration and invasion assays. *Mutat Res* 2013;**752**:10–24.
36. Ludwig RJ, Boehme B, Podda M, Henschler R, Jager E, Tandi C, et al. Endothelial P-selectin as a target of heparin action in experimental melanoma lung metastasis. *Cancer Res* 2004;**64**:2743–50.
37. Erpenbeck L, Schön MP. Deadly allies: the fatal interplay between platelets and metastasizing cancer cells. *Blood* 2010;**115**:3427–36.
38. Coupland LA, Chong BH, Parish CR. Platelets and P-selectin control tumor cell metastasis in an organ-specific manner and independently of NK cells. *Cancer Res* 2012;**72**:4662–71.
39. Yan HH, Pickup M, Pang Y, Gorska AE, Li Z, Chytil A, et al. Gr-1^{+}CD11b^{+} myeloid cells tip the balance of immune protection to tumor promotion in the premetastatic lung. *Cancer Res* 2010;**70**:6139–49.
40. Ahn GO, Brown JM. Matrix metalloproteinase-9 is required for tumor vasculogenesis but not for angiogenesis: role of bone marrow-derived myelomonocytic cells. *Cancer Cell* 2008;**13**:193–205.